Cerebello-Basal Ganglia Network Global Efficiency Predicts Cortical Network Global Efficiency

T. Bryan Jackson[a], Jessica A. Bernard[a,b]

[a]Department of Psychological and Brain Sciences, Texas A&M University

[b]Texas A&M Institute for Neuroscience, Texas A&M University

Corresponding author:

T. Bryan Jackson

Department of Psychological and Brain Sciences

Texas A&M University, 4235 TAMU

College Station, TX 77843

Email: bjackson@tamu.edu

Acknowledgements

Portions of this research were conducted with the advanced computing resources provided by Texas A&M High Performance Research Computing.

Funding information: Brain and Behavior Research Foundation, Grant/Award Number: NARSAD Young Investigator Award, Donald and Janet; National Institute on Aging, Grant/Award Number: R01AG064010-01

Abstract

The cerebellum (CB) and basal ganglia (BG) each have distinct functional subregions that are interconnected via disynaptic trans-thalamic pathways and interact with functionally connected cortical regions through discrete thalamic loops. Previous work shows functional connectivity between these phylogenetically ancient regions is topographically organized with high levels of interconnectedness (Hausman et al., 2019). It has been posited that this subcortical network provides the foundation from which cortical systems emerge, spanning cognitive, emotional, and motor domains, implying subcortical network measures are strongly related to cortical network measures (Bostan & Strick, 2018); however, it is currently unknown how differences in network measures within the subcortical network relates to differences within cortical networks. Here, rsfMRI data from 233 non-related, right-handed participants (Human Connectome Project-1200) were selected to test whether subcortical network interconnectedness predicted within-network interconnectedness in the cortex. 70 regions of interest comprising the CB-BG and canonical cortical resting-state networks (default mode, central executive, salience, motor, and emotional) were defined based on previous work. Network-level global efficiency (GE) in the CB-BG network positively predicted GE in all 5 cortical networks. When looking at network segregation, relationships were seen only when looking at the CB-BG network and cortical motor network. We also replicated previous findings showing a high degree of CB-BG interconnectedness in a large sample. This work has implications for understanding cortical network organization and cortical-subcortical interactions in healthy adults and may help in deciphering subcortical changes seen in disease states.

Keywords: cerebellum; basal ganglia; subcortical networks; default mode network; global efficiency; fMRI; Human Connectome Project

Introduction

Until recently, the cerebellum (CB), basal ganglia (BG), and the networks they form with one another have been relatively understudied outside of the realms of motor behavior and learning. However, the CB, BG, and their associated computations are phylogenetically ancient (Bell, 2002; Grillner & Robertson, 2016; Herrick M.D., 1924; Smeets et al., 2000; Stephenson-Jones et al., 2012) and support a wide array of animal behaviors that are associated with cortical function, including human verbal, emotional, and cognitive abilities (Chen & Desmond, 2005; Guell et al., 2018; for reviews, see Ward et al., 2013 and Schmahmann, 2019). Throughout mammalian evolution, the CB scaled in size with the neocortex; however, CB volume relative to neocortical volume is expanded in great apes and humans (Balsters et al., 2010; Barton & Venditti, 2014). Human studies have shown a substantial increase in projections to the CB from prefrontal regions compared to that of macaques (Ramnani et al., 2006) and larger neocortically-linked CB lobules (Crus I and Crus II) compared to other CB lobules (Balsters et al., 2010). Likewise, primate BG regions, particularly the striatum, are volumetrically larger in relation to the neocortex when compared to insectivores and other earlier mammals (Stephan & Andy, 1964), and striatal regions (particularly the ventral portion) are known to be anatomically and functionally linked with regions of the cortex associated with higher order processing (i.e. dorsolateral prefrontal cortex) in humans (Di Martino et al., 2008; Draganski et al., 2008). With this in mind, it stands to reason that CB and BG processing is inherently linked to cortically-associated cognitive processing, potentially acting as nodes in a larger network (Bostan & Strick, 2018); however, direct investigations of the relationships between subcortical and cortical network interactions remain rare. Here, we provide

further evidence for a CB-BG functional network and investigate its role in scaffolding cortical function.

Originally described in non-human primates, the CB and BG each have distinct subregions that are connected to corresponding cortical regions through separate, closed-loop, trans-thalamic pathways (Kelly & Strick, 2003, 2004), providing a neural mechanism for the long-range communication needed for subcortically-supported cortical processing. Historically, the CB and BG were associated with separate learning functions and were thought to perform calculations independent of each other: the BG were associated with reward and reinforcement-learning paradigms (reviewed in Lee, Seo, & Jung, 2012), while the CB was associated with prediction and error-correcting processes (reviewed in Wolpert et al., 2011). However, non-human primate work has demonstrated evidence of direct, bidirectional subcortical CB-BG communication circuits (Bostan et al., 2010; Hoshi et al., 2005). This subcortical network consists largely of di-synaptic second-order neuronal pathways: one that projects from the dentate nucleus of the CB to the thalamus, then terminates primarily in the striatum of the BG (Hoshi et al., 2005), and another that projects from the subthalamic nucleus of the BG to the pontine nucleus, then terminates in multiple cerebellar regions (Bostan et al., 2010).

Evidence from *in vivo* studies of the human brain parallel these findings. For example, motor-associated CB and BG nodes and cognition-associated regions of the CB and BG are functionally connected with one another at rest (Hausman, Jackson, Goen, & Bernard, 2019) and diffusion tractography details similar subthalamic connections seen in animals (Pelzer et al., 2013). This coupled with evidence from viral tract tracing (Bostan et al., 2010) and other human functional connectivity (Bernard et al., 2012, 2013) studies suggest that cortico-CB and cortico-BG networks are not only the separate, bi-directional loops as once thought, but are also pathways

in a larger, highly-integrated learning and computational network (Bostan & Strick, 2018), perhaps serving a foundational role in cognitive processes in humans.

Insights from across both neurological and psychiatric disease states also support the potential importance of effective CB-BG integration. Patients with Parkinson's disease, known primarily for the deterioration of motor-related dopaminergic neurons in the substantia nigra (DeLong & Wichmann, 2010), show changes within the CB (Wu & Hallett, 2013) and its networks (Caligiore et al., 2016), and CB hyperactivity has been associated with resting tremors (Asanuma, 2006). Wang et al. (2011) found stronger motor-related CB and BG activity in those with Tourette's Syndrome (compared to healthy controls). Those with schizophrenia show differences in the cortico-striatal- thalamo-cerebellar tract connecting the CB and BG to the cortex (Anticevic et al., 2014; Ji et al., 2019), Purkinje cells within the CB (Mavroudis et al., 2017), and dopaminergic circuits within the BG (Mehler-Wex et al., 2006). These differences are thought to be related to the dysfunction in cognitive and information processing found in those with schizophrenia. Cortico-thalamo-CB circuits have been implicated in dystonia (Argyelan et al., 2009), long thought to be a BG-related disorder, and mouse models have shown that normalizing aberrant CB output to the BG can reduce symptoms of dystonia (Neychev et al., 2008). Even in healthy aging, there are aberrations in the CB-BG circuit (Hausman et al., 2019) and differences in connectivity within the closed-loop cortico-thalamo circuits of both the CB and BG (Bernard et al., 2013; Bo et al., 2014; Griffanti et al., 2018).

Given the phylogenetic age of the CB and BG and their involvement in multiple cortical networks and disease states (Bostan & Strick, 2018), it has been posited that these regions may be important support structures, providing scaffolding for cortical regions and networks (Bostan & Strick, 2018). fMRI is a useful way to look at intrinsic brain organization and has implications for

understanding function (Karahanoğlu & Van De Ville, 2017), so researchers regularly use behaviorally associated resting-state functional networks as an additional means of investigating functional brain organization. These networks largely overlap with task positive regions that are engaged during behavioral performance (e.g. cingulo-opercular network – CO; fronto-parietal network - FP; Fair et al., 2009). In contrast, the default mode network (DMN) is not associated with any task behavior, but instead with self-directed thought and internal mentation (Buckner et al., 2008; Fair et al., 2009; Fox et al., 2015). We posit that if cortical networks are built upon a foundation of CB-BG interactions, then a measures of CB-BG network interconnectedness would predict measures of cortical interconnectedness.

Graph theoretical approaches are useful in quantifying connectivity patterns and thus determining the interconnectedness of a given network. To quantify interconnectedness, we calculated network-level global efficiency (GE) for the CB-BG network and 5 canonical resting-state networks. GE is a graph theory metric defined as the average inverse shortest path length and was designed to capture the efficiency of information transmission within a given network (Rubinov & Sporns, 2010; Sporns et al., 2004; Whitfield-Gabrieli & Nieto-Castanon, 2012). It is currently unknown how subcortical CB-BG functional connectivity network interconnectedness relates to cortical functional connectivity network interconnectedness; however, we hypothesize that the CB and BG each provide a foundation for cortical processing, consistent with the assertions of Bostan and Strick (2018), and thus predict that an increase in CB-BG resting-state network network-level GE would correlate positively with default mode and task-positive network network-level GE. We further investigated other graph theoretical measures computed by the CONN toolbox (Whitfield-Gabrieli & Nieto-Castanon, 2012) such as cost and average path length in an exploratory fashion to compare the findings of each. We were also interested in network

segregation, a measure that quantifies how disconnected the nodes in a network are from nodes in the global network that has been shown to be important to healthy brains (Chan et al., 2014). Given our theory that the CB-BG network is foundation to cortical networks, we predicted CB-BG network segregation would correlate positively with cortical network segregation. Last, we also replicated previous work detailing CB-BG network connectivity patterns (Hausman et al., 2019).

Methods

Participants – HCP

Preprocessed resting-state functional MRI (rsfMRI) data from the S1200 Release of Human Connectome Project (WU-UMN HCP Consortium) were downloaded for analysis. Onlydata for unrelated, right-handed individuals without psychiatric diagnoses were used. Data were considered for this study only if the participant displayed right-handedness (Handedness>24), attained a high school degree (SSAGA_Educ>11), reported no family history of mental illness (FamHist_*_None = 1), did not meet the DSM4 criteria for Alcohol Abuse or Dependence (SSAGA_Alc_D4_Ab_Dx != 5; SSAGA_Alc_D4_Dp_Dx != 5), and did not meet the DSM criteria for Marijuana Dependence (SSAGA_Mj_Ab_Dep = 0). To account for any potential familial similarities in brain structure and function, only one participant from each family unit was chosen. Using Excel's Rand() function, each participant was assigned a random number and the participant with the largest number in their family was selected for inclusion in the analyses. Only participants with a complete set of data (one T1w structural and four resting-state fMRI sessions with the associated movement parameters) were used for analysis. These exclusions resulted in a sample size of 233 individuals ranging in age from 22 to 37 years (111 males, 122 females; see Supplemental Text 1). Detailed descriptions of each variable used to eliminate participants are

available here: https://wiki.humanconnectome.org (see HCP Data Dictionary Public- Updated for the 1200 Subject Release).

HCP image acquisition and preprocessing

rsfMRI data for each participant consisted of four 15-minute runs collected over 2 sessions (1200 volumes, 720 ms TR, 2 mm isotropic voxels; see Van Essen et al. (2012) for full details on fMRI acquisition). Preprocessed T1w structural, functional, and motion regressor data were downloaded from the HCP S1200 Release Amazon Web Services repository. Details of the preprocessing pipeline for functional images are fully described in Glasser et al. (2013). Structural scans had undergone gradient distortion correction, bias field correction, and registration to the 0.8 mm resolution MNI brain using Multimodal Surface Matching (Glasser et al., 2013, 2016). Additionally, structural images underwent tissue type segmentation and functional images underwent smoothing (5 mm FWHM) and artifact detection (global signal z-value threshold: 5, subject motion threshold: 0.9 mm) using the CONN toolbox (v. 19b; Whitfield-Gabrieli & Nieto-Castanon, 2012), a Matlab-based application designed for functional connectivity analysis. CONN was used with MATALB R2019a on centOS 7. Data were then denoised using confound regressors for 5 temporal components each from the segmented CSF and white matter, 24 motion realignment parameters, signal and/or motion outliers, and the 1st order derivative from the effect of rest. Finally, data underwent linear detrending and bandpass filtering (0.008 - 0.09 Hz).

Regions of interest

3.5 mm spherical, binarized regions of interest (ROIs) representing a rsfMRI network of CB and BG nodes (CB-BG network), 4 separate cortical rsfMRI networks and 1 limbic rsfMRI network were created with coordinates from previous works using fslmaths (FSL v.6.0.3: FMRIB's Software Library, www.fmrib.ox.ac.uk/fsl; Jenkinson, Beckmann, Behrens, Woolrich, & Smith,

2012). CB-BG network ROIs were created using CB and BG coordinates previously used in our recent work (Hausman et al., 2019). ROIs from two task-related resting-state networks, the cingulo-opercular (CO) and the fronto-parietal (FP), and the default mode network (DMN) were created using coordinates originally reported by Fair et al. (2009). Cortical motor network (MN) ROIs were created using coordinates based on Mayka, Corcos, Leurgans, & Vaillancourt (2006). Limbic ROIs (here termed "emotional network" - EN) were created using coordinates originally reported by Stein et al. (2007) and adapted using information from Deen, Pitskel, & Pelphrey, (2011). Importantly, regions of the CB and BG have been associated with cortical and limbic networks, especially the MN; however, the networks chosen here did not include ROIs from within the CB or BG. This allowed us to directly correlate measures from the CB-BG network to measures from the cortical and limbic networks. To account for the use of both left and right ROIs in some cortical networks, all lateralized (defined as more than 3mm from the midline in the x direction) ROIs without a reported contralateral match were mirrored in the x direction (see Supplemental Table 1 for parallel analysis using only the original ROIs). Table 1 and

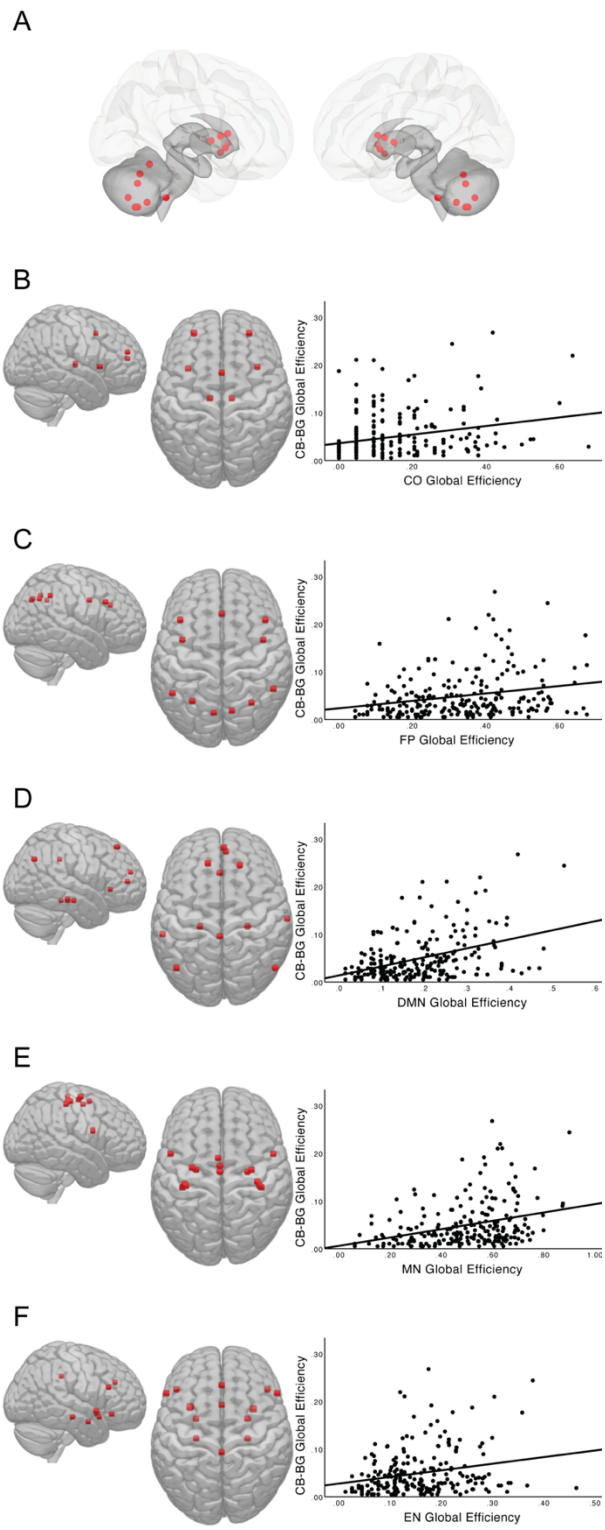

Figure 1 provide details for the 70 resulting ROIs. ROIs will be referred to by their abbreviation in Table 1 from this point forward.

Figure 1. ROI locations and scatterplots depicting the relationship between A) the CB-BG network and each of the cortical networks, B) CO, C) FP, D), DMN, E) MN, F) EN.

Table 1. Abbreviations, region names, MNI coordinates, netw
in the analyses. All ROIs are 3.5mm, spherical, and binarized.
using its contralateral pair.

Abbreviation	Region	MNI (X, Y, Z)	Network	Source
L VSi	Left inferior ventral striatum	- 9, 9, -8	CB-BG	Hausman, Jackson, 2019
R VSi	Right inferior ventral striatum	9, 9, -8	CB-BG	*Mirrored*
L VSs	Left superior ventral striatum	-10, 15, 0	CB-BG	Hausman, Jackson, 2019
R VSs	Right superior ventral striatum	10, 15, 0	CB-BG	*Mirrored*
L DC	Left dorsal caudate	-13, 15, 9	CB-BG	Hausman, Jackson, 2019
R DC	Right dorsal caudate	13, 15, 9	CB-BG	*Mirrored*
L DCP	Left dorsal caudal putamen	-28, 1, 3	CB-BG	Hausman, Jackson, 2019
R DCP	Right dorsal caudal putamen	28, 1, 3	CB-BG	*Mirrored*
L DRP	Left dorsal rostral putamen	-25, 8, 6	CB-BG	Hausman, Jackson, 2019
R DRP	Right dorsal rostral putamen	25, 8, 6	CB-BG	*Mirrored*
L VRP	Left ventral rostral putamen	-20, 12, -3	CB-BG	Hausman, Jackson, 2019
R VRP	Right ventral rostral putamen	20, 12, -3	CB-BG	*Mirrored*
R LobV	Right Cerebellar Lobule V	16, -52, -17	CB-BG	Hausman, Jackson, 2019
L LobV	Left Cerebellar Lobule V	-16, -52, -17	CB-BG	*Mirrored*
R LobVI	Right Cerebellar Lobule VI	26, -60, -25	CB-BG	Hausman, Jackson, 2019
L LovVI	Left Cerebellar Lobule VI	-26, -60, -25	CB-BG	*Mirrored*
R CrusI	Right Cerebellar CrusI	47, -61, -34	CB-BG	Hausman, Jackson, 2019
L Crus I	Left Cerebellar CrusI	-47, -61, -34	CB-BG	*Mirrored*
R CrusII	Right Cerebellar CrusII	41, -70, -46	CB-BG	Hausman, Jackson, 2019
L CrusII	Left Cerebellar CrusII	-41, -70, -46	CB-BG	*Mirrored*
L dlPFC	Left dorsolateral prefrontal cortex	-43, 22, 34	FP	Fair et al. 2009
R dlPFC	Right dorsolateral prefrontal cortex	43, 22, 34	FP	Fair et al. 2009
L FG	Left frontal gyrus	-41, 3, 36	FP	Fair et al. 2009
R FG	Right frontal gyrus	41, 3, 36	FP	Fair et al. 2009
mCC	Medial cingulate cortex	0, 29, 30	FP	Fair et al. 2009
L IPL	Left inferior parietal lobule	-51, -51, 36	FP	Fair et al. 2009
R IPL	Right inferior parietal lobule	51, -47, 42	FP	Fair et al. 2009
L IPS	Left intraparietal sulcus	-31, -59, 42	FP	Fair et al. 2009
R IPS	Right intraparietal sulcus	30, -61, 39	FP	Fair et al. 2009
L Precun	Left precuneus	-9, -72, 37	FP	Fair et al. 2009

R Precun	Right precuneus	10, -69, 39	FP	Fair et al. 2009
L aPFC	Left anterior prefrontal cortex	-28, 51, 1	CO	Fair et al. 2009
R aPFC	Right anterior prefrontal cortex	27, 50, 23	CO	Fair et al. 2009
L aI	Left anterior insula	-35, 14, 5	CO	Fair et al. 2009
R aI	Right anterior insula	36, 16, 4	CO	Fair et al. 2009
dACC	Dorsal anterior cingulate cortex	-1, 10, 46	CO	Fair et al. 2009
L aTh	Left anterior Thalamus	-12, -15, 7	CO	Fair et al. 2009
R aTh	Right anterior Thalamus	10, -15, 8	CO	Fair et al. 2009
amPFC	Anterior medial prefrontal cortex	1, 54, 21	DMN	Fair et al. 2009
vmPFC	Ventromedial prefrontal cortex	-3, 29, -2	DMN	Fair et al. 2009
L SFC	Left superior frontal cortex	-14, 38, 52	DMN	Fair et al. 2009
R SFC	Right superior frontal cortex	17, 37, 52	DMN	Fair et al. 2009
L ITL	Left inferior temporal lobe	-61, -33, -15	DMN	Fair et al. 2009
R ITL	Right inferior temporal lobe	65, -17, -15	DMN	Fair et al. 2009
L Para(DMN)	Left parahippocampus	-22, -26, -16	DMN	Fair et al. 2009
L Para(DMN)	Right parahippocampus	25, -26, -14	DMN	Fair et al. 2009
pCC	Posterior cingulate cortex	-2, -36, 37	DMN	Fair et al. 2009
L lPFC	Left lateral prefrontal cortex	-47, -67, 36	DMN	Fair et al. 2009
R lPFC	Right lateral prefrontal cortex	53, -67, 36	DMN	Fair et al. 2009
retsplen	Retro Splenial	3, 51, 8	DMN	Fair et al. 2009
supCC	Supragenual cingulate	0, 34, 30	EN	Stein et al. 2007
subCC	Subgenual cingulate	0, 15, -14	EN	Stein et al. 2007
L OFC	Left orbitofrontal cortex	-46, 31, -9	EN	Stein et al. 2007
R OFC	Right orbitofrontal cortex	46, 31, -9	EN	*Mirrored*
L Para(EN)	Left parahippocampus gyrus	-26, -19, -14	EN	Stein et al. 2007
L Para(EN)	Right parahippocampus gyrus	26, -19 -14	EN	*Mirrored*
L lPFC	Left lateral prefrontal cortex	-56, 26, 25	EN	Stein et al. 2007
R lPFC	Right lateral prefrontal cortex	56, 26, 25	EN	*Mirrored*
L Amyg	Left amygdala	-26, 0, -20	EN	Stein et al. 2007
R Amyg	Right amygdala	26, 0, -20	EN	*Mirrored*
pCC	Posterior cingulate cortex	0, -33, 38	EN	Stein et al. 2007
L vaI	Left ventral anterior insula	-33, 13, -7	EN	Deen et al., 2011
R vaI	Right ventral anterior insula	32, 10, -6	EN	Deen et al., 2011
mPMC	Mesial prefrontal cortex	-3 -5 60	MN	Mayka 2006
pSMA	pre-supplementary motor area	-4 3 59	MN	Mayka 2006
SMA	Supplementary motor area	-3 -11 61	MN	Mayka 2006
L lPMC	Left lateral premotor cortex	-26 -10 62	MN	Mayka 2006
R lPMC	Right lateral premotor cortex	25, -11, 61	MN	*Mirrored*
L dlPMC	Left dorsolateral premotor cortex	-30 -8 64	MN	Mayka 2006
R dlPMC	Right dorsolateral premotor cortex	29 -9 64	MN	*Mirrored*
L vlPMC	Left ventral lateral premotor cortex	-52 7 22	MN	Mayka 2006

R vlPMC	Right ventral lateral premotor cortex	52 6 21	MN	*Mirrored*
L SMC	Left sensorimotor cortex	-39 -24 59	MN	Mayka 2006
R SMC	Right sensorimotor cortex	38 -25 59	MN	*Mirrored*
L M1	Left primary motor cortex	-37 -25 64	MN	Mayka 2006
R M1	Right primary motor cortex	36 -21 58	MN	*Mirrored*
L S1	Left primary sensorimotor cortex	-40 -27 54	MN	Mayka 2006
R S1	Right primary sensorimotor cortex	39 -28 54	MN	*Mirrored*

fMRI participant-level correlation matrices

For each participant, a timeseries for each of the 70 ROIs was extracted and cross-correlated using bivariate analyses, resulting in a correlation matrix (70x70) for each participant. All participant-level analyses were performed in the CONN toolbox (v. 19b; Whitfield-Gabrieli & Nieto-Castanon, 2012).

Subcortical network analysis – replication

Subcortical ROIs originally used in our recent investigation of CB-BG connectivity in young and older adults (Hausman et al. 2019) were used to replicate the findings in a larger sample, again computed using the CONN toolbox (v. 19b; Whitfield-Gabrieli & Nieto-Castanon, 2012). Bivariate correlations were calculated by cross correlating each timeseries of four lateralized CB ROIs (R CrusI, R CrusII, R LobV, and R LobVI) and six lateralized BG ROIs (L VSi, L VSs, L VRP, L DRP, L DC, L DCP). Fisher z-transformed correlation matrices were computed and thresholded at p(FDR) = .05.

Graph theory and correlational analyses

Average network-level graph theoretical measures were computed separately for each of the six networks within the CONN toolbox (Whitfield-Gabrieli & Nieto-Castanon, 2012). Edges were defined as thresholded correlation coefficients ($\beta > .1$) and nodes were defined as the ROIs in a given network (Fair et al., 2009). Given previous findings that show a high degree of interconnectedness within each network (Fair et al., 2009; Geerligs et al., 2015; Hausman et al.,

2019; Stein et al., 2007), we focused on network-level GE, a measure of how efficiently information in a network travels, as the primary measure of each network's interconnectedness for our analyses here (Achard & Bullmore, 2007; Latora & Marchiori, 2001; Sheffield et al., 2016; Whitfield-Gabrieli & Nieto-Castanon, 2012). To test whether the GE of the CB-BG network was related to the GE of the FP, CO, DMN, EN, or MN, bivariate Pearson correlations were performed between the CB-BG network and each of the other networks (i.e., CB-BG GE compared to FP GE) using IBM SPSS 25 (IBM Corporation Armonk, NY, 2017). We also calculated the following network-level graph theoretical measures and performed the same analyses in order to compare the findings in an exploratory manner: betweenness centrality (average of the number of times each node is part of a shortest-path between any two ROIs), cost/degree (average of the proportion/number of edges that are connected to a given node - for our purposes, cost and degree are redundant measures and are discussed as one), and average path length (average number of edges traversed from ROI-to-ROI). For a full mathematical description of each of these measures and of GE, please see Achard & Bullmore, 2007; Latora & Marchiori, 2001; Rubinov & Sporns, 2010; Sporns et al., 2004 and Whitfield-Gabrieli & Nieto-Castanon, 2012. Bonferroni corrections were applied to all exploratory correlations.

Network segregation analysis

Participant-level Fisher z-transformed correlation matrices were used to calculate within-network and between-network connectivity separately for each network (Chan et al., 2014). Within-network connectivity was defined as the average z-score for all ROI-to-ROI connections in a network. Between-network connectivity was defined differently for the CB-BG and cortical networks. For the CB-BG network, between-network connectivity was defined as the average z-score of the ROI-to-ROI connections between nodes in the CB-BG network and nodes in all other

networks. For all cortical networks, between-network connectivity was defined as the average z-score of the ROI-to-ROI connections between all nodes a cortical network and the nodes in every other cortical network (leaving out the CB-BG network). Next, network segregation was calculated

separately for each network using the following formula:

$$\frac{Zwithin - Zbetween}{Zwithin}$$

To answer the question of whether subcortical segregation predicted cortical segregation, Pearson bivariate correlations were performed between the CB-BG and each cortical network's segregation score.

Results

CB-BG connectivity network

Table 2 lists *t*-scores and beta values for each ROI-to-ROI pair in the lateralized CB-BG network analysis, performed to replicate our previous findings in a larger sample (Hausman et al., 2019). Broadly speaking, these results successfully replicate our past work showing robust positive connectivity between the CB and BG. Notably, these analyses did reveal 2 anticorrelations that were not seen in our prior work (Hausman et al., 2019). These anticorrelations were seen between R CrusII and both L VSi and L VRP. We suspect however, that the anticorrelations found here may be due to higher sensitivity and statistical power associated with the larger sample used in this investigation.

Table 2. β values and paired *t*-tests and for each significant ROI-ROI pair.

ROI pairs	β	*t* (222)	*p* (FDR)
R CrusI - R CrusII	0.07	12.81	p < 0.001
R CrusI - R LobV	0.01	2.88	p = .007
R CrusI -R LobVI	0.02	5.12	p < 0.001
R CrusI - L VSi	0.01	2.64	p = .01
R CrusI - L VRP	0.02	6.16	p < 0.001
R CrusI - L DC	0.02	5.76	p < 0.001
R CrusII - R LobV	0.01	2.96	p = .006
R CrusII - R LobVI	0.01	4.25	p < 0.001
R CrusII - L VSs	0.01	2.83	p = .008
R CrusII - L VSi	-0.01	-2.16	p = .04
R CrusII - L VRP	-0.01	-2.78	p = .009
R CrusII - L DC	0.01	4.04	p < 0.001
R LobV - R LobVI	0.02	7.35	p < 0.001
R LobV - L DRP	0.01	3.31	p = 0.002
R LobV - L DCP	0.02	5.77	p < 0.001
R LobVI - L VSs	0.01	2.36	p = .03
R LobVI - L VSi	0.01	2.22	p = .03
R LobVI - L VRP	0.01	2.98	p = .005
R LobVI - L DRP	0.02	5.25	p < 0.001
R LobVI - L DCP	0.01	4.37	p < 0.001
R LobVI - L DC	0.02	4.45	p < 0.001
L VSs - L VSi	0.03	10.13	p < 0.001
L VRP - L VSs	0.07	16.96	p < 0.001
L VRP - L VSi	0.05	12.90	p < 0.001
L VRP - L DC	0.08	18.00	p < 0.001
L DRP - L VSs	0.03	8.02	p < 0.001
L DRP - L VSi	0.01	4.05	p < 0.001
L DRP - L VRP	0.11	24.45	p < 0.001
L DRP - L DC	0.05	13.85	p < 0.001
L DCP - L VSs	0.01	3.48	p = 0.001
L DCP - L VRP	0.06	15.93	p = 0.002
L DCP - L DRP	0.12	26.71	p = 0.005
L DCP - L DC	0.03	8.01	p = 0.006
L DC - L VSs	0.05	12.08	p = 0.03
L DC - L VSi	0.02	7.47	p = 0.04

Subcortical-cortical graph theory network-level correlations

Table 3. Pearson correlation values (*r's)* for each subcortical-cortical pairing.

	FP	CO	DMN	MN	EN
Global Efficiency	**.241*** **	**.252*** **	**.401*** **	**.314*** **	**.228*** **
Segregation	**-.01**	**.03**	**-.07**	**.18***	**-.07**
Betweenness Centrality	0.054	.185	.231***	0.038	0.108
Cost/Degree	.284***	.268***	.410***	.351***	.251***
Avg Path Length	0.015	0.103±	.142	-0.033	0.027

Note. Significance for main analyses (bolded) was assessed at p < .05. Exploratory analyses were assessed using a Bonferroni-corrected p-value of p = .003.
***$p < .001$ **$p < .01$ *$p < .05$ ± $n < 233$.

Table 3 lists Pearson correlation coefficients (r) for relationships between CB-BG and cortical network GE and Figure 1 depicts the scatterplots for each correlation. Positive correlations were found between the CB-BG network and every cortical network (FP: $r(221) = .24$, $p < .001$; CO: $r(221) = .25$, $p < .001$; DMN: $r(221) = .40$, $p < .001$; MN: $r(221) = .31$, $p < .001$; EN: $r(221) = .23$, $p < .001$), indicating a relationship between the interconnectedness of the CB-BG network and that of the cortical and limbic networks.

The additional exploratory correlations between CB-BG and cortical/limbic graph theory measures that survived Bonferroni correction ($p < .003$) are also presented in Table 3. Cost and degree paralleled the GE results with correlations of similar magnitude (FP: $r(221) = .28$, $p < .001$; CO: $r(221) = .27$, $p < .001$; DMN: $r(221) = .41$, $p < .001$; MN: $r(221) = .35$, $p < .001$; EN: $r(221) = .25$, $p < .001$). Betweenness centrality of the CB-BG network was positively associated with that in the DMN ($r(221) = .23$, $p < .001$). No other subcortical-cortical correlations were found when using betweenness centrality or average path length as the measure of interest ($rs < .19$).

Correlation analyses between the original networks (containing no mirrored ROIs) are presented in Supplemental Table 1. Fewer correlations were present overall, and even fewer

survived after we applied a Bonferroni correction to all tests ($p < .0025$). CB-BG GE and cost/degree only correlated with that of the DMN, with no other significant correlations found. Finally, for a complete picture of cortical network interconnectedness, exploratory correlational analyses between cortical and limbic networks are presented in Supplemental Table 2. The GE of each network was corelated with that of every other network,

with the exception of the FP/MN and FP/EN correlations.

Network segregation

Table 3 lists Pearson correlation coefficients (r) for relationships between CB-BG and cortical network segregation and Figure 2 depicts the scatterplot for the significant correlations. CB-BG and MN segregation was positively correlated, $r(221) = .18$, $p < .01$ (Figure 2). No other significant correlations between the CB-BG network segregation and that of the other networks were found (Table 3). Additionally, no correlations were found between any cortical network, indicating that segregation is not related across cortical networks (Supplemental Table 3).

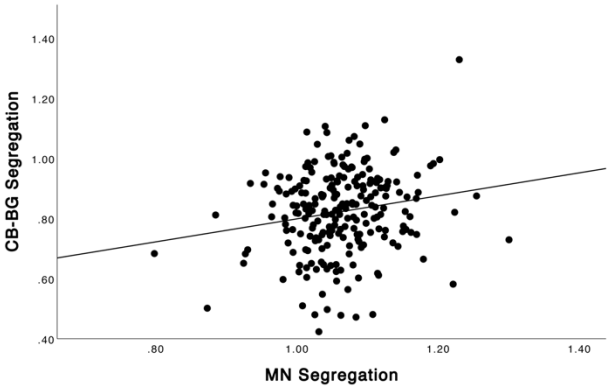

Figure 2. Scatterplot depicting the relationship between the segregation of the CB-BG network and of the MN.

Discussion

Here, we performed a novel correlational analysis relating CB-BG network interconnectedness to cortical network interconnectedness to investigate the relationships between the CB-BG subcortical network and cortical networks, as posited by Bostan & Strick (2018). We found that network properties detailing the degree of interconnectedness (GE, cost/degree) show similarities between the CB-BG and cortical networks, providing support that the CB and BG act

as nodes in larger networks spanning the cortex. This work has implications for understanding cortical network organization and cortical-subcortical interactions in healthy adults and may help in understanding the broad network-based changes seen in disease states.

Lateralized CB-BG functional connectivity replication

First and foremost, we replicated our previous work (Hausman et al., 2019) investigating CB-BG connectivity at rest and report strong connectivity between these subcortical regions. While the general pattern of findings is consistent with our prior work demonstrating robust connectivity between the CB and the BG, this replication revealed several new findings as well. Within the CB, we found associations between every lateralized node, unlike in our prior work where we did not find an association between R CrusII and R LobV. Although seemingly minor, this indicates that the functional signals within the CB at rest may be more similar than previously shown, even in regions associated with different behavioral domains (cognitive versus motor, respectively) and cortical circuits (Balsters et al., 2010, 2013; Bernard et al., 2012). A similar pattern again emerged within the BG: broadly speaking, ROIs within the BG are functionally connected as previously detailed, though additional within-BG connections were revealed (L DRP-L VSs, L DCP – L VSi, and L DCP- L DC), likely due to increased power stemming from the larger sample size used here. Between CB and BG nodes, we again largely replicated our previous findings. Expanding on our prior work, we also found that R LobVI is functionally connected to every BG ROI, reflecting R LobVI's role in both motor and cognitive function (Balsters et al., 2013) and the functional connections to premotor, motor, and prefrontal area (Bernard et al., 2012). However, we also found anticorrelations for R CrusII - L VSi and R CrusII - L VRP connections. This is potentially indicative of delayed or lagged communication between these regions but best

interpretation of negative relationships between time courses is up for debate (Meszlényi et al., 2017) and warrants further study into the nature of CB-BG communication.

CB-BG GE and segregation analyses

Participants with high CB-BG network GE tended to have high cortical network GE, as we predicted given the high degree of anatomical interconnectedness the subcortical regions have with each other and with cortical systems (Bostan & Strick, 2018). This suggests that the CB and BG are each foundational regions that together serve specialized computational roles in larger cortical networks underlying cognition. Existing evidence from studies of psychopathology suggest this circuit plays an important role in certain disease states. For example, Ji et al. (2019) found more changes in connectivity in cortico-striatal-cerebellar circuits in those with schizophrenia than in healthy controls, with higher-order associative circuits displaying hypo-connectivity while sensory-motor areas displayed hyper-connectivity. Importantly, these differences correlated with cognitive dysfunction, furthering the argument that the CB-BG network supports cognitive function associated with cortical regions. The DMN, FP, and CO also show differences in patients with schizophrenia (Manoliu et al., 2013) but the relationships between the interconnectedness of these networks is as of yet unknown. Moreover, bipolar disorder (Anticevic et al., 2014) and Parkinson's disease (Caligiore et al., 2016) display dysfunctional connectivity patterns between the cortex, the thalamus, and the CB-BG, further highlighting the potential importance of this subcortical scaffolding. Notably, such differences in connectivity are present across other disorders, but an exhaustive discussion is beyond the scope of the work here. Exploring the CB-BG relationship and their cortical projections within the context of psychopathologies would be interesting and worthwhile. We would expect larger cortical and limbic network dysfunction in

diseases or states of aberrant CB-BG network dysfunction, which is consistent with what we see in the broader literature (Anticevic et al., 2014; Ji et al., 2019).

Additionally, a supplemental analysis found that the only network pairs that had uncorrelated GE were the FP-EN and FP-MN (Supplemental Table 2). Previous work by Fermin et al. (2016) investigating activation of cortico-striato-thalamo-cortical circuits during a sequence learning paradigm found evidence of distinct sub-circuits differentiated by learning stage. Limbic (EN) and motor (MN) circuits, phylogenetically much older than the cognitive loops (Balsters et al., 2010; Stephenson-Jones et al., 2011, 2012), were activated in early and late learning, respectively, with cognitive circuits associated with the intermediate stage prior to automaticity. These differences coupled with the patterns found here lead us to speculate that the SN and DMN are scaffolded similarly to the FP and we posit that the EN, non-motor cortical networks (FP, SN, DMN), and MN are each separately supported by the CB-BG network. Alternatively, positive correlations between cortical network GE may be indicative of between-network communication of related networks at the cortical level; however, the correlations between cortical systems were generally smaller than those between the CB-BG network and cortical networks, adding further support for CB-BG scaffolding.

Interestingly, CB-BG segregation from the cortical nodes predicted MN segregation from cortical nodes, but no other relationship with cortical segregation was found. Chan et al. (2014) found a negative linear relationship between sensory-motor region segregation and age; however, cortical network segregation and age was better explained by a quadradic relationship, showing a sharp decline in segregation around the age of 50. Due to the age of the sample used here (18-36), there simply may not have been enough variability in segregation scores in the non-motor cortical and limbic areas resulting in the lack of a relationship with the CB-BG network. Alternatively,

since the CB and BG are each involved in a variety of behaviors and associated networks, it may be that the sub-regions of each show different patterns of segregation, though we did not investigate this possibility here. Lastly, we did not find a relationship in network segregation measures between any of the cortical networks. It may be that network segregation is not a good descriptor of these relationships in healthy young adults and, given the age-related changes previously noted (Chan et al., 2014), warrants further exploration in older adult populations.

Exploratory graph theory metrics

To further understand the relationships between the CB-BG network and cortical networks, parallel exploratory analyses were conducted using other graph theory measures. Cost and degree analyses fully replicated the main GE analysis, showing qualitatively larger correlations between every measure (see Table 3). This was generally expected, as these are measures of the number of connections in a network and are proxies for network efficiency (Rubinov & Sporns, 2010). Betweenness centrality, a measure of the average proportion of times that an ROI in a network is part of the shortest ROI-to-ROI path within the network (Rubinov & Sporns, 2010), showed a relationship between the CB-BG network and both the SN and DMN. Finally, average path length only related the CB-BG network with the DMN. This was unexpected, as the average path length and betweenness centrality are both similar in conception to GE (Rubinov & Sporns, 2010). It may be that not all in-network ROIs are connected, resulting in ROIs with zero efficiency being left out of the equation and thus failing to fully capture the efficiency of the network. GE solves this issue by including ROI connections that have zero efficiency, as opposed to average path length and betweenness centrality, and provides further support for using GE in our analyses. Together, these exploratory findings help to confirm the idea that subcortical connectivity is related to network

measures of large-scale cortical networks, though the degree to which this is the case varies by measure.

Limitations

While this work provides important new insights into the interplay between subcortical CB-BG networks and those in the cortex, there are several limitations to consider. For each network, we used unequal number of ROIs that represent a subset of the possible ROIs that could be used to investigate these networks. These choices were rooted in the literature of canonical resting-state networks (Deen et al., 2011; Fair et al., 2009; Mayka et al., 2006; Stein et al., 2007) but accounting for the disparate number of regions, using a whole-brain parcellation approach, or defining ROIs within a network using a more data-driven method may produce different results and warrant their own studies. Future studies may also benefit from simply increasing the number of ROIs, allowing for higher resolution when capturing network measures. Relatedly, we also did not distinguish between the ventral and dorsal attention systems and additional ROIs would help decipher any differences between the organization of those systems and relationships with the CB-BG network. Additionally, although there are CB and BG nodes known to be involved in many of the cortical resting-state networks, the cortical networks chosen to be used here did not include any CB or BG ROIs so that we could directly compare CB-BG and cortical network patterns. While necessary for our purposes, this method inherently truncates the size of the functional networks to only cortical nodes, potentially limiting the accuracy of the network measure in the context of how these networks are recruited during task processing. Lastly, we used classic time-series autocorrelational analyses to build an ROI-to-ROI table. Other methods that can account for temporal lag like dynamic time warping (Meszlényi 2017) or sliding window analyses may reveal additional details

about the temporal order of activation in within-network ROI relationships that are used to calculate the graph theory measures.

Conclusions

These findings suggest CB-BG network interconnectedness is related to cortical network interconnectedness, in support of theories suggesting that the CB and BG each serve a foundational role for learning and cognition in support of cortical networks (Bostan & Strick, 2018). We also showed that, while regions associated with similar behavioral domains (cognitive, motor, etc.) tend to be highly functionally connected (Bernard et al., 2013; Hausman et al., 2019), CB and BG subregions are generally highly functionally connected, even between regions associated with different behavioral domains and cortical circuits. These findings detail network dynamics in a large representative sample and may help to elucidate network-related changes in clinical or older adult populations in the future.

References

Achard, S., & Bullmore, E. (2007). Efficiency and Cost of Economical Brain Functional Networks. *PLoS Computational Biology*, *3*(2), e17. https://doi.org/10.1371/journal.pcbi.0030017

Anticevic, A., Cole, M. W., Repovs, G., Murray, J. D., Brumbaugh, M. S., Winkler, A. M., Savic, A., Krystal, J. H., Pearlson, G. D., & Glahn, D. C. (2014). Characterizing Thalamo-Cortical Disturbances in Schizophrenia and Bipolar Illness. *Cerebral Cortex*, *24*(12), 3116–3130. https://doi.org/10.1093/cercor/bht165

Argyelan, M., Carbon, M., Niethammer, M., Ulug, A. M., Voss, H. U., Bressman, S. B., Dhawan, V., & Eidelberg, D. (2009). Cerebellothalamocortical Connectivity Regulates Penetrance in Dystonia. *Journal of Neuroscience*, *29*(31), 9740–9747. https://doi.org/10.1523/JNEUROSCI.2300-09.2009

Asanuma, K. (2006). Network modulation in the treatment of Parkinson's disease. *Brain*, *129*(10), 2667–2678. https://doi.org/10.1093/brain/awl162

Balsters, J. H., Cussans, E., Diedrichsen, J., Phillips, K. A., Preuss, T. M., Rilling, J. K., & Ranganath, C. (2010). Evolution of the cerebellar cortex: The selective expansion of prefrontal-projecting cerebellar lobules. *NeuroImage*, *49*(3), 2045–2052. https://doi.org/10.1016/j.neuroimage.2009.10.045

Balsters, J. H., Whelan, C. D., Robertson, I. H., & Ramnani, N. (2013). Cerebellum and cognition: Evidence for the encoding of higher order rules. *Cerebral Cortex*, *23*(6), 1433–1443. https://doi.org/10.1093/cercor/bhs127

Barton, R. A., & Venditti, C. (2014). Rapid Evolution of the Cerebellum in Humans and Other

Great Apes. *Current Biology*, *24*(20), 2440–2444. https://doi.org/10.1016/j.cub.2014.08.056

Bell, C. C. (2002). *Evolution of Cerebellum-Like Structures*. *2002*, 312–326.

Bernard, J. A., Peltier, S. J., Wiggins, J. L., Jaeggi, S. M., Buschkuehl, M., Fling, B. W., Kwak, Y., Jonides, J., Monk, C. S., & Seidler, R. D. (2013). Disrupted cortico-cerebellar connectivity in older adults. *NeuroImage*, *83*, 103–119. https://doi.org/10.1016/j.neuroimage.2013.06.042

Bernard, J. A., Seidler, R. D., Hassevoort, K. M., Benson, B. L., Welsh, R. C., Wiggins, J. L., Jaeggi, S. M., Buschkuehl, M., Monk, C. S., Jonides, J., & Peltier, S. J. (2012). Resting state cortico-cerebellar functional connectivity networks: a comparison of anatomical and self-organizing map approaches. *Frontiers in Neuroanatomy*, *6*(August), 1–19. https://doi.org/10.3389/fnana.2012.00031

Bo, J., Lee, C.-M., Kwak, Y., Peltier, S. J., Bernard, J. A., Buschkuehl, M., Jaeggi, S. M., Wiggins, J. L., Jonides, J., Monk, C. S., & Seidler, R. D. (2014). Lifespan Differences in Cortico-Striatal Resting State Connectivity. *Brain Connectivity*, *4*(3), 166–180. https://doi.org/10.1089/brain.2013.0155

Bostan, A. C., Dum, R. P., & Strick, P. L. (2010). The basal ganglia communicate with the cerebellum. *Proceedings of the National Academy of Sciences*, *107*(18), 8452–8456. https://doi.org/10.1073/pnas.1000496107

Bostan, A. C., & Strick, P. L. (2018). The basal ganglia and the cerebellum: Nodes in an integrated network. *Nature Reviews Neuroscience*, *19*(6), 338–350. https://doi.org/10.1038/s41583-018-0002-7

Buckner, R. L., Andrews-Hanna, J. R., & Schacter, D. L. (2008). The Brain's Default Network. *Annals of the New York Academy of Sciences*, *1124*(1), 1–38. https://doi.org/10.1196/annals.1440.011

Caligiore, D., Helmich, R. C., Hallett, M., Moustafa, A. A., Timmermann, L., Toni, I., & Baldassarre, G. (2016). Parkinson's disease as a system-level disorder. *Nature Publishing Group Parkinson's Disease*, *2*(1), 16025. https://doi.org/10.1038/npjparkd.2016.25

Chan, M. Y., Park, D. C., Savalia, N. K., Petersen, S. E., & Wig, G. S. (2014). Decreased segregation of brain systems across the healthy adult lifespan. *Proceedings of the National Academy of Sciences*, *111*(46), E4997–E5006. https://doi.org/10.1073/pnas.1415122111

Chen, S. H. A., & Desmond, J. E. (2005). Temporal dynamics of cerebro-cerebellar network recruitment during a cognitive task. *Neuropsychologia*, *43*(9), 1227–1237. https://doi.org/10.1016/j.neuropsychologia.2004.12.015

Deen, B., Pitskel, N. B., & Pelphrey, K. A. (2011). Three Systems of Insular Functional Connectivity Identified with Cluster Analysis. *Cerebral Cortex*, *21*(7), 1498–1506. https://doi.org/10.1093/cercor/bhq186

DeLong, M., & Wichmann, T. (2010). Changing Views of Basal Ganglia Circuits and Circuit Disorders. *Clinical EEG and Neuroscience*, *41*(2), 61–67. https://doi.org/10.1177/155005941004100204

Di Martino, A., Scheres, A., Margulies, D. S., Kelly, A. M. C., Uddin, L. Q., Shehzad, Z., Biswal, B., Walters, J. R., Castellanos, F. X., & Milham, M. P. (2008). Functional Connectivity of Human Striatum: A Resting State fMRI Study. *Cerebral Cortex*, *18*(12), 2735–2747. https://doi.org/10.1093/cercor/bhn041

Draganski, B., Kherif, F., Kloppel, S., Cook, P. A., Alexander, D. C., Parker, G. J. M., Deichmann, R., Ashburner, J., & Frackowiak, R. S. J. (2008). Evidence for Segregated and Integrative Connectivity Patterns in the Human Basal Ganglia. *Journal of Neuroscience*, *28*(28), 7143–7152. https://doi.org/10.1523/JNEUROSCI.1486-08.2008

Fair, D. A., Cohen, A. L., Power, J. D., Dosenbach, N. U. F., Church, J. A., Miezin, F. M., Schlaggar, B. L., & Petersen, S. E. (2009). Functional Brain Networks Develop from a "Local to Distributed" Organization. *PLoS Computational Biology*, *5*(5), e1000381. https://doi.org/10.1371/journal.pcbi.1000381

Fermin, A. S. R., Yoshida, T., Yoshimoto, J., Ito, M., Tanaka, S. C., & Doya, K. (2016). Model-based action planning involves cortico-cerebellar and basal ganglia networks. *Scientific Reports*, *6*(1), 31378. https://doi.org/10.1038/srep31378

Fox, K. C. R., Spreng, R. N., Ellamil, M., Andrews-Hanna, J. R., & Christoff, K. (2015). The wandering brain: Meta-analysis of functional neuroimaging studies of mind-wandering and related spontaneous thought processes. *NeuroImage*, *111*, 611–621. https://doi.org/10.1016/j.neuroimage.2015.02.039

Geerligs, L., Renken, R. J., Saliasi, E., Maurits, N. M., & Lorist, M. M. (2015). A Brain-Wide Study of Age-Related Changes in Functional Connectivity. *Cerebral Cortex*, *25*(7), 1987–1999. https://doi.org/10.1093/cercor/bhu012

Glasser, M. F., Smith, S. M., Marcus, D. S., Andersson, J. L. R., Auerbach, E. J., Behrens, T. E. J., Coalson, T. S., Harms, M. P., Jenkinson, M., Moeller, S., Robinson, E. C., Sotiropoulos, S. N., Xu, J., Yacoub, E., Ugurbil, K., & Van Essen, D. C. (2016). The Human Connectome Project's neuroimaging approach. *Nature Neuroscience*, *19*(9), 1175–1187.

https://doi.org/10.1038/nn.4361

Glasser, M. F., Sotiropoulos, S. N., Wilson, J. A., Coalson, T. S., Fischl, B., Andersson, J. L., Xu, J., Jbabdi, S., Webster, M., Polimeni, J. R., Van Essen, D. C., & Jenkinson, M. (2013). The minimal preprocessing pipelines for the Human Connectome Project. *NeuroImage*, *80*, 105–124. https://doi.org/10.1016/j.neuroimage.2013.04.127

Griffanti, L., Stratmann, P., Rolinski, M., Filippini, N., Zsoldos, E., Mahmood, A., Zamboni, G., Douaud, G., Klein, J. C., Kivimäki, M., Singh-Manoux, A., Hu, M. T., Ebmeier, K. P., & Mackay, C. E. (2018). Exploring variability in basal ganglia connectivity with functional MRI in healthy aging. *Brain Imaging and Behavior*, *12*(6), 1822–1827. https://doi.org/10.1007/s11682-018-9824-1

Grillner, S., & Robertson, B. (2016). The Basal Ganglia Over 500 Million Years. *Current Biology*, *26*(20), R1088–R1100. https://doi.org/10.1016/j.cub.2016.06.041

Guell, X., Gabrieli, J. D. E., & Schmahmann, J. D. (2018). Triple representation of language, working memory, social and emotion processing in the cerebellum: convergent evidence from task and seed-based resting-state fMRI analyses in a single large cohort. *NeuroImage*, *172*(August 2017), 437–449. https://doi.org/10.1016/j.neuroimage.2018.01.082

Hausman, H. K., Jackson, T. B., Goen, J. R. M., & Bernard, J. A. (2019). From Synchrony to Asynchrony: Cerebellar–Basal Ganglia Functional Circuits in Young and Older Adults. *Cerebral Cortex*, *41*(18), 5255–5281. https://doi.org/10.1093/cercor/bhz121

Herrick M.D., C. J. (1924). Origin and Evolution of the Cerebellum. *Archives of Neurology and Psychiatry*, *11*(6), 621–652.

Hoshi, E., Tremblay, L., Féger, J., Carras, P. L., & Strick, P. L. (2005). The cerebellum communicates with the basal ganglia. *Nature Neuroscience*, *8*(11), 1491–1493. https://doi.org/10.1038/nn1544

Jenkinson, M., Beckmann, C. F., Behrens, T. E. J., Woolrich, M. W., & Smith, S. M. (2012). FSL. *NeuroImage*, *62*(2), 782–790. https://doi.org/10.1016/j.neuroimage.2011.09.015

Ji, J. L., Diehl, C., Schleifer, C., Tamminga, C. A., Keshavan, M. S., Sweeney, J. A., Clementz, B. A., Hill, S. K., Pearlson, G., Yang, G., Creatura, G., Krystal, J. H., Repovs, G., Murray, J., Winkler, A., & Anticevic, A. (2019). Schizophrenia Exhibits Bi-directional Brain-Wide Alterations in Cortico-Striato-Cerebellar Circuits. *Cerebral Cortex*, *29*(11), 4463–4487. https://doi.org/10.1093/cercor/bhy306

Karahanoğlu, F. I., & Van De Ville, D. (2017). Dynamics of large-scale fMRI networks: Deconstruct brain activity to build better models of brain function. *Current Opinion in Biomedical Engineering*, *3*, 28–36. https://doi.org/10.1016/j.cobme.2017.09.008

Kelly, R. M., & Strick, P. L. (2003). Cerebellar Loops with Motor Cortex and Prefrontal Cortex of a Nonhuman Primate. *The Journal of Neuroscience*, *23*(23), 8432–8444. https://doi.org/10.1523/JNEUROSCI.23-23-08432.2003

Kelly, R. M., & Strick, P. L. (2004). Macro-architecture of basal ganglia loops with the cerebral cortex: use of rabies virus to reveal multisynaptic circuits. In *Brain* (pp. 447–459). https://doi.org/10.1016/S0079-6123(03)43042-2

Latora, V., & Marchiori, M. (2001). Efficient Behavior of Small-World Networks. *Physical Review Letters*, *87*(19), 198701. https://doi.org/10.1103/PhysRevLett.87.198701

Lee, D., Seo, H., & Jung, M. W. (2012). Neural basis of reinforcement learning and decision making. *Annual Review of Neuroscience*, *35*, 287–308. https://doi.org/10.1146/annurev-neuro-062111-150512

Manoliu, A., Riedl, V., Doll, A., Bäuml, J. G., Mühlau, M., Schwerthöffer, D., Scherr, M., Zimmer, C., Förstl, H., Bäuml, J., Wohlschläger, A. M., Koch, K., & Sorg, C. (2013). Insular Dysfunction Reflects Altered Between-Network Connectivity and Severity of Negative Symptoms in Schizophrenia during Psychotic Remission. *Frontiers in Human Neuroscience*, *7*(May), 1–16. https://doi.org/10.3389/fnhum.2013.00216

Mavroudis, I. A., Petrides, F., Manani, M., Chatzinikolaou, F., Ciobică, A. S., Pădurariu, M., Kazis, D., Njau, S. N., Costa, V. G., & Baloyannis, S. J. (2017). Purkinje cells pathology in schizophrenia. A morphometric approach. *Romanian Journal of Morphology and Embryology = Revue Roumaine de Morphologie et Embryologie*, *58*(2), 419–424. http://www.ncbi.nlm.nih.gov/pubmed/28730225

Mayka, M. A., Corcos, D. M., Leurgans, S. E., & Vaillancourt, D. E. (2006). Three-dimensional locations and boundaries of motor and premotor cortices as defined by functional brain imaging: A meta-analysis. *NeuroImage*, *31*(4), 1453–1474. https://doi.org/10.1016/j.neuroimage.2006.02.004

Mehler-Wex, C., Riederer, P., & Gerlach, M. (2006). Dopaminergic dysbalance in distinct basal ganglia neurocircuits: Implications for the pathophysiology of parkinson's disease, schizophrenia and attention deficit hyperactivity disorder. *Neurotoxicity Research*, *10*(3–4), 167–179. https://doi.org/10.1007/BF03033354

Meszlényi, R. J., Hermann, P., Buza, K., Gál, V., & Vidnyánszky, Z. (2017). Resting State fMRI

Functional Connectivity Analysis Using Dynamic Time Warping. *Frontiers in Neuroscience*, *11*(FEB), 1–17. https://doi.org/10.3389/fnins.2017.00075

Neychev, V. K., Fan, X., Mitev, V. I., Hess, E. J., & Jinnah, H. A. (2008). The basal ganglia and cerebellum interact in the expression of dystonic movement. *Brain*, *131*(9), 2499–2509. https://doi.org/10.1093/brain/awn168

Pelzer, E. A., Hintzen, A., Goldau, M., von Cramon, D. Y., Timmermann, L., & Tittgemeyer, M. (2013). Cerebellar networks with basal ganglia: feasibility for tracking cerebello-pallidal and subthalamo-cerebellar projections in the human brain. *European Journal of Neuroscience*, *38*(8), 3106–3114. https://doi.org/10.1111/ejn.12314

Ramnani, N., Behrens, T. E. J., Johansen-Berg, H., Richter, M. C., Pinsk, M. A., Andersson, J. L. R., Rudebeck, P., Ciccarelli, O., Richter, W., Thompson, A. J., Gross, C. G., Robson, M. D., Kastner, S., & Matthews, P. M. (2006). The Evolution of Prefrontal Inputs to the Cortico-pontine System: Diffusion Imaging Evidence from Macaque Monkeys and Humans. *Cerebral Cortex*, *16*(6), 811–818. https://doi.org/10.1093/cercor/bhj024

Rubinov, M., & Sporns, O. (2010). Complex network measures of brain connectivity: Uses and interpretations. *NeuroImage*, *52*(3), 1059–1069. https://doi.org/10.1016/j.neuroimage.2009.10.003

Schmahmann, J. D. (2019). The cerebellum and cognition. *Neuroscience Letters*, *688*(April 2018), 62–75. https://doi.org/10.1016/j.neulet.2018.07.005

Sheffield, J. M., Kandala, S., Burgess, G. C., Harms, M. P., & Barch, D. M. (2016). Cingulo-opercular Network Efficiency Mediates the Association Between Psychotic-like Experiences and Cognitive Ability in the General Population. *Biological Psychiatry:*

Cognitive Neuroscience and Neuroimaging, *1*(6), 498–506. https://doi.org/10.1016/j.bpsc.2016.03.009

Smeets, W. J. A. J., Marín, O., & González, A. (2000). Evolution of the basal ganglia: New perspectives through a comparative approach. *Journal of Anatomy*, *196*(4), 501–517. https://doi.org/10.1017/S0021878299006007

Sporns, O., Chialvo, D., Kaiser, M., & Hilgetag, C. (2004). Organization, development and function of complex brain networks. *Trends in Cognitive Sciences*, *8*(9), 418–425. https://doi.org/10.1016/j.tics.2004.07.008

Stein, J. L., Wiedholz, L. M., Bassett, D. S., Weinberger, D. R., Zink, C. F., Mattay, V. S., & Meyer-Lindenberg, A. (2007). A validated network of effective amygdala connectivity. *NeuroImage*, *36*(3), 736–745. https://doi.org/10.1016/j.neuroimage.2007.03.022

Stephan, H., & Andy, O. J. (1964). Quantitative Comparisons of Brain Structures from Insectivores to Primates. *American Zoologist*, *4*(1), 59–74.

Stephenson-Jones, M., Ericsson, J., Robertson, B., & Grillner, S. (2012). Evolution of the basal ganglia: Dual-output pathways conserved throughout vertebrate phylogeny. *The Journal of Comparative Neurology*, *520*(13), 2957–2973. https://doi.org/10.1002/cne.23087

Stephenson-Jones, M., Samuelsson, E., Ericsson, J., Robertson, B., & Grillner, S. (2011). Evolutionary conservation of the basal ganglia as a common vertebrate mechanism for action selection. *Current Biology*, *21*(13), 1081–1091. https://doi.org/10.1016/j.cub.2011.05.001

Van Essen, D. C., Ugurbil, K., Auerbach, E., Barch, D., Behrens, T. E. J., Bucholz, R., Chang,

A., Chen, L., Corbetta, M., Curtiss, S. W., Della Penna, S., Feinberg, D., Glasser, M. F., Harel, N., Heath, A. C., Larson-Prior, L., Marcus, D., Michalareas, G., Moeller, S., … Yacoub, E. (2012). The Human Connectome Project: A data acquisition perspective. *NeuroImage*, *62*(4), 2222–2231. https://doi.org/10.1016/j.neuroimage.2012.02.018

Wang, Z., Maia, T. V., Marsh, R., Colibazzi, T., Gerber, A., & Peterson, B. S. (2011). The Neural Circuits That Generate Tics in Tourette's Syndrome. *American Journal of Psychiatry*, *168*(12), 1326–1337. https://doi.org/10.1176/appi.ajp.2011.09111692

Ward, P., Seri And, S., & Cavanna, A. E. (2013). Functional neuroanatomy and behavioural correlates of the basal ganglia: Evidence from lesion studies. *Behavioural Neurology*, *26*(4), 219–223. https://doi.org/10.3233/BEN-2012-120264

Whitfield-Gabrieli, S., & Nieto-Castanon, A. (2012). Conn : A Functional Connectivity Toolbox for Correlated and Anticorrelated Brain Networks. *Brain Connectivity*, *2*(3), 125–141. https://doi.org/10.1089/brain.2012.0073

Wolpert, D. M., Diedrichsen, J., & Flanagan, J. R. (2011). Principles of sensorimotor learning. *Nature Reviews Neuroscience*, *12*(12), 739–751. https://doi.org/10.1038/nrn3112

Wu, T., & Hallett, M. (2013). The cerebellum in Parkinson's disease. *Brain*, *136*(3), 696–709. https://doi.org/10.1093/brain/aws360

Supplemental Text

1. 100610, 101309, 102614, 102715, 102816, 103111, 103818, 104012, 104416, 105014, 105115, 105216, 105620, 105923, 106016, 106824, 107422, 108020, 108121, 108323, 108525, 109325, 109830, 111009, 111312, 111413, 111716, 112314, 112516, 112920, 113215, 113922, 114621, 114823, 114924, 115017, 116726, 117122, 118124, 118730, 118831, 119126, 119732, 119833, 120414, 120515, 121416, 122317, 122620, 123521, 123925, 124422, 125222, 126426, 126628, 127630, 127832, 128026, 128632, 128935, 129028, 129331, 129634, 130114, 130316, 130417, 130619, 130821, 131217, 132017, 132118, 133019, 133928, 134223, 134627, 135225, 136833, 137027, 137532, 138130, 138332, 138837, 140319, 143426, 144125, 144832, 145127, 146129, 146533, 149741, 149842, 150423, 151324, 151425, 151728, 151930, 152427, 153126, 153227, 153833, 154229, 154734, 156031, 156233, 156334, 156536, 157437, 157942, 159239, 159744, 161630, 162228, 162733, 163432, 164030, 164131, 164939, 167036, 167440, 168139, 169545, 172029, 172332, 172433, 172534, 173435, 173738, 173940, 174841, 175742, 176542, 177241, 178142, 178849, 178950, 179245, 180230, 180533, 180735, 180836, 182739, 182840, 185442, 185846, 186040, 188145, 189349, 189450, 190031, 191033, 192136, 195041, 195647, 196346, 198249, 198855, 199352, 202113, 204016, 204420, 206323, 206727, 208125, 211114, 211316, 212015, 212217, 213522, 214423, 219231, 220721, 236130, 245333, 275645, 281135, 285446, 286650, 287248, 299760, 304020, 309636, 310621, 311320, 314225, 316633, 321323, 329844, 336841, 349244, 350330, 358144, 361941, 381543, 385046, 391748, 397154, 397760, 414229, 419239, 459453, 468050, 510225, 516742, 529549, 529953, 547046, 552241, 561949, 567759, 571144, 580751, 589567, 618952, 622236, 675661, 680250, 680452, 748662, 757764, 789373, 835657, 849264, 97998

Supplemental Table 1. Pearson Correlation values for each subcortical-cortical pairing.

	FP	CO	DMN	MN	EN
Global Efficiency	0.123	0.161	.325***	0.180	0.122
Betweenness Centrality	0.079	0.053	0.015	-0.008	-0.011
Cost/Degree	0.159	0.174	.355***	0.174	0.189
Avg Path Length	0.076	-0.024	-0.061	0.037	0.051

Note: Analyses were assessed using a Bonferroni-corrected p-value of p = .0025. ***$p < .001$ **$p < .01$ *$p < .05$

Supplemental Table 2. Pearson Correlation values showing the relationship between each cortical network's global efficiency.

	FP	CO	DMN	MN	EN
FP	1	.242***	.197**	.156	0.166
CO	.242***	1	.289***	.252***	.176**
DMN	.197**	.289***	1	.303***	.239***
MN	.156	.252***	.303***	1	.299***
EN	0.166	.176**	.238***	.299***	1

Note: Analyses were assessed using a Bonferroni-corrected p-value of p = .005. ***$p < .001$ **$p < .01$ *$p < .05$

Supplemental Table 3. Pearson Correlation values showing the relationship between each cortical network's segregation.

	FP	CO	DMN	MN	EN
FP	1	.00	-.01	-.05	-.05
CO	.00	1	.01	.07	.-.02
DMN	-.01	.01	1	.09	-.01
MN	-.05	.07	.09	1	.05
EN	-.05	-.02	-.01	.05	1

Note: Analyses were assessed using a Bonferroni-corrected p-value of p = .005. ***$p < .001$ **$p < .01$ *$p < .05$